Assessment of the Integration Strategy between GPS and Body-Worn MEMS Sensors with Application to Sports

Adrian Waegli, Dr. Jan Skaloud, Dr. Phillip Tomé, Jean-Marie Bonnaz
École polytechnique Fédérale de Lausanne, Switzerland

BIOGRAPHY

Adrian Waegli obtained a M.Sc. in Geomatics Engineering from EPF Lausanne, Switzerland for his work on the ionospheric corrections of EGNOS. After working as a surveyor at the Swiss Federal Office of Topography, he joined the Geodetic Engineering Laboratory of EPFL in 2004 as Ph.D. student. His research focuses on the integration of satellite and inertial navigation systems for performance analysis in sports.

Jan Skaloud is a scientist and lecturer at the Institute of Geomatics at EPF Lausanne, Switzerland. He holds a Ph.D. and M.Sc. in Geomatics Engineering from the University of Calgary and Dipl. Ing. in Surveying Engineering from the Czech Institute of Technology, Prague. He has been involved with the GPS research and development since 1993 and has worked extensively on the integration of GPS and inertial navigation systems for precise airborne and terrestrial mapping.

Phillip Tomé holds a Ph.D. in surveying engineering from the University of Porto, Portugal, and a M.Sc. in electronics engineering. There, he got specialized for the integration of inertial and satellite navigation systems for aircraft attitude determination. Currently, he is working as scientific collaborator at EPFL, in the field of sensors integration for navigation purposes.

Jean-Marie Bonnaz studied surveying Engineering at ESGT Le Mans, France. He currently prepares his diploma theses at EPFL on the properties of MEMS-IMU for trajectory analysis.

ABSTRACT

This paper describes experiments that were performed involving a professional downhill skier equipped with a low-cost L1 GPS receiver and a MEMS-IMU composed of 3 single axis gyroscopes, accelerometers and magnetometers. In addition, the skier carried an L1/L2 GPS receiver and a tactical-grade IMU (LN200). The experiments aimed to assess the navigation performance of different GPS/MEMS-IMU integration strategies compared to high-quality GPS/INS integration. After presenting an overview of currently applied integration methods, the unscented Kalman filter approach was compared to the extended Kalman filter approach in loosely coupled mode. The relevance of the simple MEMS-IMU sensor error model was verified by comparing the filter output to the reference data.

INTRODUCTION

Nowadays, the performance analysis of athletes is based on simple chronometry and video recordings. GPS measurement methods allow the accurate recording of position, velocity and derived acceleration, which opens new possibilities for continuous comparison of athletes' performance throughout a racecourse [1].

Unfortunately, the accuracy of GPS is limited by the high dynamics of sports (e.g. ski racing, car racing, rowing). Quick changes of the satellites constellation render the carrier-phase ambiguity resolution difficult or even impossible. To overcome the lack of continuity in the GPS signals and to observe accelerations and orientations, inertial and magnetic sensors are integrated with GPS. While motorsports can benefit from the traditional GPS/INS instrumentation [2], the ergonomic constraints of some sports (e.g. ski racing) urge to use devices based on Micro-Electro-Mechanical System (MEMS) technology. Due to their small size, low cost and power consumption, MEMS sensors are suitable for trajectory analysis in sports where ergonomics plays an important role. In addition, because of their cost and size, dual-frequency GPS receivers will be restricted to few disciplines with higher accuracy demands.

In [3], we introduced a L1 GPS/MEMS-IMU system that provides encouraging results for the performance evaluation in sports (RMS of 0.5m in the position, 0.2m/s for the velocity and 2° for the orientation determination). Furthermore, it has been shown that such integration was capable to bridge GPS gaps of up to 10s without significant accuracy degradation. Nevertheless, the GPS/MEMS-IMU integration strategy based on an extended Kalman filter (EKF) and the inertial error model are revised in this paper.

Firstly, we investigate alternatives to the EKF that might be more appropriate to use considering the high dynamics of some sports. Indeed, the first-order approximation of the EKF may yield insufficiently accurate results for high non-linearities. After discussing some alternatives, we first study the implementation of sigma-point filters which by principle does not require the approximation by linearization. Secondly, the error model of the MEMS-IMU is analyzed. The pertinence of sensor modeling is verified experimentally by means of reference signals (tactical-grade IMU and carrier-phase DGPS positioning).

GPS/INS INTEGRATION STRATEGY TRADEOFF

EKF is widely used in GPS/INS integration. Although it has proven its effectiveness with higher-grade inertial sensors, its dependency on correct (physical) models, the underlying Gaussian assumption and linearization somewhat limits its use when working with MEMS sensors. The linearization independency might be a crucial factor in sports because of the high dynamics endured in some disciplines. In addition, the fast convergence of the filter is crucial as the motion of the athletes may change rapidly (e.g. after the start). In the following, we revise different integration strategies and discuss their operation with the sports application (Table 1).

	EKF	PF	SPKF	AI	Importance for the sports application
Linearization dependency	☹	☺	☺	☺	high
Model dependency	☹	☹	☹	☺	medium
Prior knowledge dependency	☹	☹	☹	☺	medium
Sensor dependency	☹	☹	☹	☺	low
Parameter tuning/training	human	human	human	self	low
Computational cost	☺	☹	☺	☹	medium
Convergence	☺	😐	☺	☹	high
Appropriateness for sports	😐	☹	☺	☹	

Table 1: Comparison of different GPS/INS integration strategies for the sports applications

Linearization Dependency

In conventional GPS/INS integration the state distribution of the EKF is approximated by a Gaussian random variable which is then propagated analytically through the (first-order) linearization of the non-linear system. In contrast, particle filters (PF) and sigma-point KF (SPKF) propagate the state covariance accurately (for the SPKF at least to the second-order). Hence, the prediction mode can be improved. Unlike EKF and SPKF, PFs make no assumption on the probability density function (PDF) and might show a superior numerical accuracy to other filtering methods. However, they are computationally expensive for high-dimensional systems with large sampling rates.
The derivation of Jacobians for system and measurement models required in EKF is nontrivial and may lead to significant implementation difficulties. Furthermore, EKF only tolerates small errors. Otherwise, the first-order approximations may cause biased solutions and inconsistency of the covariance update which can lead to filter instability. Second order filters may correct the bias terms, but the calculation of the second order derivatives (Hessians) is nontrivial and computationally expensive. Iterative versions of KF as well require high computation power and are therefore not retained.

Model and Prior Knowledge Dependency

The KFs are based on simplified, physically meaningful error models which are established according to prior knowledge and experience. Artificial Intelligence (AI) , on the other hand, may be appropriate when the uncertainty in model structure is large, complex or vary in time – as it can be the case for MEMS sensors. Therefore, many AI-based algorithms (Artificial Neural Networks [4], neuro-fuzzy KF [5], Adaptive Neuro-Fuzzy Inference System [6]) have been developed which have sometimes shown improved error behavior compared to other filtering methods under steady conditions. On the other hand, it is questionable whether empirical models applied in AI are better suited to decorrelate signals from errors especially in cases where the varying dynamics make training sequences short and thus less appropriate. Additionally, AI methods do not use any statistical information as input, nor do they output statistics associated with the solution, unless methods of cross-validation are applied [6]. Thus, AI-based methods are not very suitable for trajectory smoothing and appear less appropriate for sports applications.

Sensor Dependency and Parameter Tuning

Tuning the measurement covariance matrix $\mathbf{R}$ and the system noise matrix $\mathbf{Q}$ of the EKF can be time-consuming and requires experience and background in both, GPS and inertial systems. The parameters may significantly vary even for sensors of similar quality. On the contrary, model-less algorithms based on AI can perform the self-following and tuning under steady

dynamics. Unfortunately, this assumption can not be satisfied in sports, where rapid filter convergence is a major criterion. In addition, adaptive KF ([7], [8]) are not retained because of the mentioned difficulty to tune the statistical models over short time periods and because of the increased computational power.

Computational Cost and Convergence

As shown in Table 1, PF are computationally expensive because of the large number of particles that need to be propagated. They are computationally too costly for high-dimensional systems and short integration times, especially in the perspective of implementing the filter in real-time. On the other hand, [9-11] have shown that the computational complexity of SPKF was equivalent to EKF ($O(n^3)$). Furthermore, this research also mentions the fast convergence of the SPKF states compared to the EKF. Therefore, and with respect to the other criteria of Table 1, SPKF seems to be the most appropriate filter candidate for our application. The implementation of both, EKF and SPKF, is presented simultaneously and their performance compared in the sequel.

SYSTEM AND OBSERVATION MODEL

Both EKF and SPKF were implemented in the local level frame (superscript n) which makes the interpretation of the state variables straightforward. The following strapdown equations need to be solved [12]:

$$\begin{bmatrix} \dot{\mathbf{r}}^n \\ \dot{\mathbf{v}}^n \\ \dot{\mathbf{R}}_b^n \end{bmatrix} = \begin{bmatrix} \mathbf{v}^n \\ \mathbf{R}_b^n \mathbf{f}^b - \left(\boldsymbol{\omega}_{in}^n + \boldsymbol{\omega}_{ie}^n\right) \times \mathbf{v}^n + \mathbf{g}^n \\ \mathbf{R}_b^n \left(\boldsymbol{\omega}_{ib}^b - \boldsymbol{\omega}_{in}^b\right) \end{bmatrix}$$

For the inertial measurements a simplified model was considered. Judging that the misalignments, drifts and constant offsets could not be decorrelated efficiently given the characteristics of the MEMS sensors and limited integration periods, only a bias term is considered. Their associated errors are modeled as first order Gauss-Markov processes:

$$\hat{\ell}^b = \ell^b + \mathbf{b}_{\ell^b} + \mathbf{w}_{\ell^b}$$
$$\dot{\mathbf{b}}_{\ell^b} = -\beta_{\ell^b} \cdot \mathbf{b}_{\ell^b} + \sqrt{2\sigma_{\ell^b}^2 \beta_{\ell^b}} \cdot \mathbf{w}_{\ell^b}$$

where $\hat{\ell}^b$ is the estimated inertial observation (specific force or rotation rate), ℓ^b the inertial measurement, $\mathbf{b}_{\ell^b}$ the bias of the inertial measurement, $\mathbf{w}_{\ell^b}$ the measurement noise, $\sigma_{\ell^b}^2$ the covariance at zero time lag and β_{ℓ^b} the inverse of the correlation time [13].

GPS positions and velocities are integrated based on a loosely coupled approach. Accounting for the lever-arm effect, the GPS position measurement model can be expressed as follows:

$$h_r\left(\hat{\mathbf{x}}_k^-\right) = \mathbf{R}_n^e \mathbf{r}_{IMU}^n + \mathbf{R}_n^e \mathbf{R}_b^n \mathbf{a}^b + \mathbf{w}_r$$

where $\mathbf{a}^b$ is the lever-arm vector between the INS center of navigation and the GPS antenna location and $\mathbf{w}_r$ the position measurement noise.

The GPS velocity measurement model needs to consider the rotation of the local level frame with respect to the body frame $\boldsymbol{\omega}_{nb}^n$:

$$h_v\left(\hat{\mathbf{x}}_k^-\right) = \mathbf{v}_{IMU}^e + \boldsymbol{\omega}_{nb}^n \times \mathbf{R}_b^n \mathbf{a}^b + \mathbf{w}_v$$

The MEMS magnetometers can be introduced as external measurements as well. However, [3] and [14] have noted that these sensors were sensitive to high frequency accelerations. [3] further pointed out that the magnetic measurements improved the orientation estimation only negligibly and thus do not affect the capacity of the MEMS sensors to bridge GPS gaps. Thus, besides during the sensor orientation initialization, the magnetometers are left aside in this investigation.

SPKF implementation aspects

In SPKF, the variance of the state is represented by a set of sigma points (SPs) whose propagation in time follow the same non-linear function as the mean value. The SPs, as well as their weights, can be chosen in various ways. The main approaches are the Central Difference Filter (CDF) and the Unscented Kalman Filter (UKF). The difference between the two methods lies in the approximation of the posterior covariance term. The CDF has a smaller absolute error in the fourth order term and also guarantees positive semi-definiteness of the posterior covariance. In contrast, the UKF can handle the non-positive semi-definiteness with two scaling parameters [15].

Because of the simplicity and limited computational cost, a Square-Root (SR) version of the UKF with non-additive error model has been implemented for this usage. This method is an adaptation of the SR-UKF [9] and the scaled unscented transformation exploited for the spreading of

the SPs [16]. The proposed algorithm chooses $n+2$ SP (n being the number of the states) that match the first two moments and that minimize the third order moments (called spherical simplex SP).

As the system model is a nonlinear function of the state and noise vector, the system noise is generated and has to go through the system process model. By augmenting the state $\mathbf{x}$ by the noise vector $\mathbf{w}$, the effect of the noise on the covariance propagation can be described naturally:

$$\mathbf{x}^a = \begin{bmatrix} \mathbf{x} \\ \mathbf{w} \end{bmatrix}, \quad \mathbf{P}^a = \begin{bmatrix} \mathbf{P} & \mathbf{0} \\ \mathbf{0} & \mathbf{Q} \end{bmatrix}$$

where superscript a indicates the augmented state. Thus, the system model with non-additive noise can be written as

$$\mathbf{x}_{k+1} = f(\mathbf{x}_k^a) \equiv f(\mathbf{x}_k, \mathbf{w}_k)$$
$$\mathbf{Q}_k = E(\mathbf{w}_k, \mathbf{w}_k)$$

In the standard UKF, the covariance $\mathbf{P}$ is computed recursively. This requires calculating the matrix square-root $\mathbf{S} \cdot \mathbf{S}^T = \mathbf{P}$ at each step (by Cholesky factorization). On the other hand, the Square-Root implementation of the UKF (SR-UKF) propagates $\mathbf{S}$ directly [10, 17]. This guarantees the positive semi-definiteness of the UKF during the covariance propagation.

Trajectory smoothing

The visibility of satellites often varies along the tracks. By processing the trajectories in forward and backward mode, the solution during periods with weak satellite constellations can be improved. The following fixed-interval smoothing algorithm combines forward and backward filtered data sets in the least squares sense:

$$\mathbf{x}_s = \mathbf{x}_f + \mathbf{P}_s \cdot \mathbf{P}_b^{-1} \left(\mathbf{x}_b^+ - \mathbf{x}_f^+ \right)$$
$$\mathbf{P}_s = \left(\mathbf{P}_f^{-1} + \mathbf{P}_b^{-1} \right)^{-1}$$

where subscript f denotes the forward, b the backward and s the smoothed solution.

EXPERIMENTAL SETUP

In order to investigate the navigation performance of the low-cost L1 GPS/MEMS-IMU setup, the instruments were mounted in a backpack together with a reference system, comprising a dual-frequency GPS receiver (Javad) and a tactical-grade IMU (LN200). Three MEMS sensors (xsens MTi) were fixed rigidly to the reference IMU with a constant lever arm (Fig. 1). A dozen of downhills of approximately 1 minute duration were performed by a professional skier. Each run was preceded by a static initialization phase of 2-3 minutes. Unfortunately, the GPS measurements of the low cost receiver (u-blox) could only be exploited for one run because its antenna was physically damaged. Therefore, the L1 measurements of the dual-frequency reference receiver were also used in the GPS/MEMS-IMU integration.

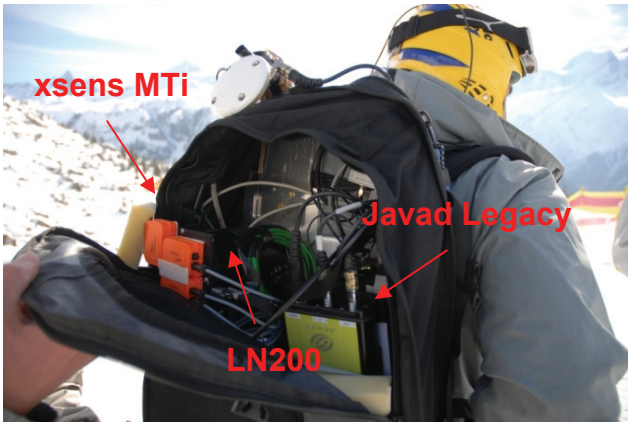

Fig. 1: Experimental Setup mounted on a professional skier

GPS/MEMS-IMU PERFORMANCE ASSESSMENT

The MEMS-IMU measurements were integrated at 100Hz with GPS position and velocity updates at 1Hz. The GPS trajectory was previously computed based on differential L1 GPS measurements with Novatel's GrafNav software. The implemented EKF and UKF solutions were then compared to the reference tracks which were determined with the dual-frequency GPS and the LN200 measurements and commercial software packages (PosProc). Table 2 compares the mean and maximum differences between 6 reference trajectories and those obtained by EKF and UKF integration of L1 GPS/MEMS-IMU integration.

The differences of the mean error are relatively small (cm-level for position, 0.3° for orientation) and are mainly driven by differential GPS accuracy (with floating ambiguities). On the other hand, the maximum errors are larger for the UKF – notably for the orientation. These maximum errors occur at the beginning or at the end of the run (Fig. 2 and Fig. 3). As soon as the filter parameters have converged the two filters provide identical results.

The covariance comparison provides similar results for both filters. This is demonstrated by plotting the covariance of the orientation and the bias during downhill 11 in Fig. 4 and Fig. 5 respectively. The covariance decreases rapidly after the start of the skier (at 10s).

From the implementation point of view, the UKF sometimes encountered problems with the positive semi-definiteness of the **S** matrix after the Cholesky update [18]. The Frobenius norm and the modified Cholesky factorization [19] helped to overcome these problems.

		EKF	UKF	Difference
RMS	N [m]	0.36	0.36	0.00
	E [m]	0.30	0.33	0.03
	h [m]	0.56	0.58	0.02
	rl [°]	0.75	0.91	0.16
	pt [°]	1.05	1.03	-0.02
	hd [°]	1.52	1.59	0.07
Max. Error	N [m]	1.01	1.05	0.04
	E [m]	0.73	1.08	0.35
	h [m]	1.20	1.39	0.19
	rl [°]	2.26	2.53	0.27
	pt [°]	2.79	2.92	0.13
	hd [°]	3.37	3.90	0.53

Table 2: Comparison of the mean and maximum errors of the EKF and UKF for 6 downhills

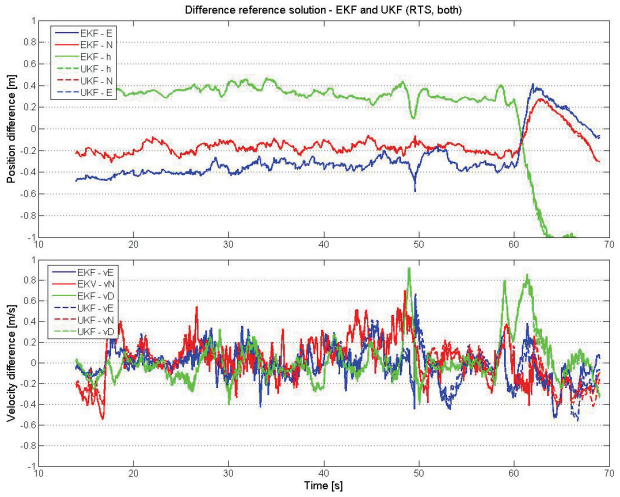

Fig. 2: Position and velocity errors of EKF and UKF during downhill #11

Furthermore, we often noticed longer computational times with the UKF compared to the EKF, even though the previously mentioned references indicate that both algorithms are $O(n^3)$ which confirms the research presented by [20]. However, the differences might come from the programming language (Matlab) where the implementation of some functions (e.g. the matrix inversion) is highly optimized, whereas others are less (SP generation, update equations, covariance reconstruction). Additionally, the EKF system matrix **F** was derived analytically which saves computational power.

Considering the increased processing time and numerical instabilities, the UKF seems to be less interesting for this application. On the other hand, the UKF remains a straightforward approach for the testing other (more complex) models (e.g. closely-coupled integration, hybridization with other sensors) and might provide better results than the EKF under different dynamics.

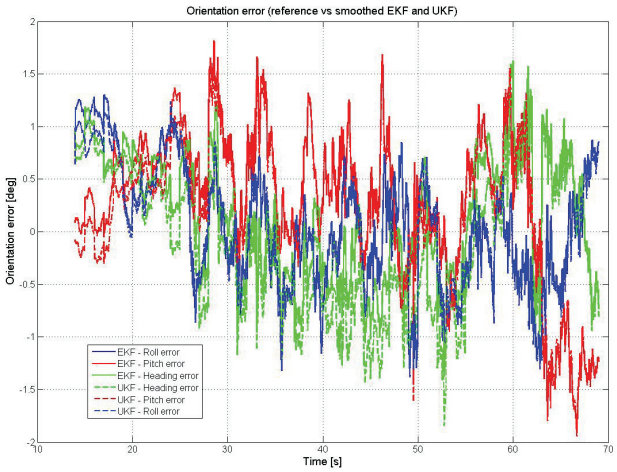

Fig. 3: Orientation error of EKF and UKF during downhill #11

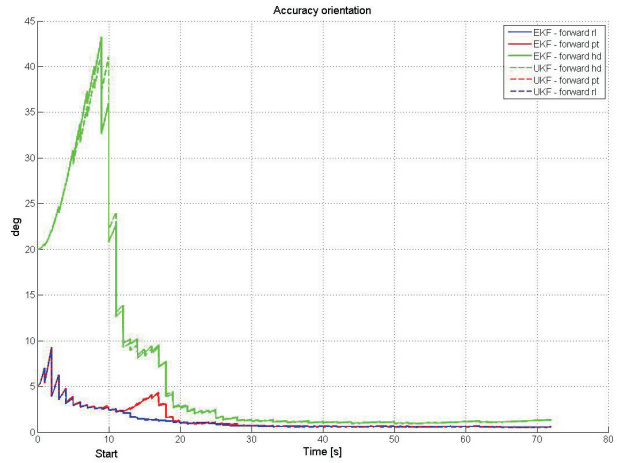

Fig. 4: Orientation covariance estimation of EKF and UKF during downhill #11

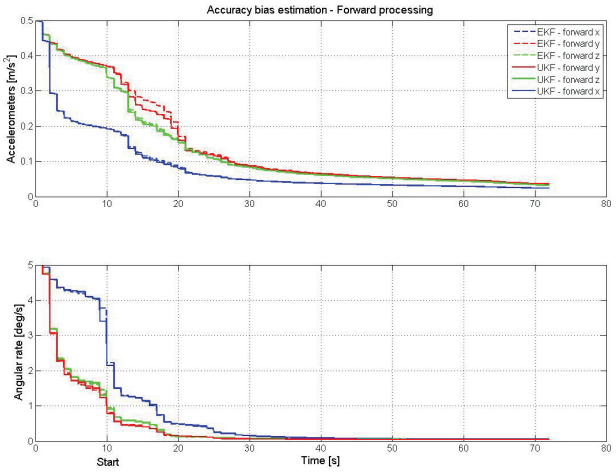

Fig. 5: Bias covariance estimation of EKF and UKF during downhill #11

MEMS-IMU ERROR MODEL INVESTIGATION

A simplified error model was considered for the inertial measurements assuming that other effects (e.g. misalignments, drifts and constant offsets) could not be efficiently decorrelated given the complexity of the MEMS sensors' error behavior. The experiments allow the direct comparison of the 3 MEMS sensors' output with the reference signals provided by the LN200. This information is also employed to verify the relevance of the MEMS error model and parameter estimation.

Firstly, in order to compare the raw measurements, the physical misalignment between the two systems had to be determined. These were estimated by feeding the EKF with the reference attitude angles provided by the reference solution (based on the LN200) using the following observation model:

$$h(\hat{\mathbf{x}}^-) = (\mathbf{I}_3 + \mathbf{B})\boldsymbol{\varphi}_{LN200} + \mathbf{w}_\varphi$$

$$\dot{\mathbf{B}} = -\beta_B \cdot \mathbf{B} + \sqrt{2\sigma_B^2 \beta_B} \cdot \mathbf{w}_\varphi$$

where $\mathbf{B}$ is the skew-symmetric form of the misalignment angles, $\boldsymbol{\varphi}_{LN200}$ are the attitude angles of the reference solution, $\mathbf{w}_\varphi$ the measurement noise and β_B the inverse of the correlation time "fixed" to infinity. The accuracy of the misalignment angles is limited by the accuracy of the MEMS orientation determination and is estimated to 0.5°.

With the reference signals corrected for the misalignment, the raw signals could be compared directly. We estimated biases b and scale factors s through parameter adjustment of the following model, assuming that drifts can be neglected for data sets of this short duration:

$$\ell_{LN200} - v = (1-s)\,\ell_{MEMS} + b$$

During the static initialization before the downhill, only biases could be computed (Fig. 6). The absence of dynamics during this period did not permit to isolate scale factors. On the other hand, during the downhills the signals decorrelated to a greater extent and the estimation of the scale factor became possible.

By comparing the biases estimated on the static portions before and after the downhills and considering that the duration of the runs does not exceed one minute, the adjustment of drifts can be neglected. For longer data sets, the correlation time could take into account sensor error drifts.

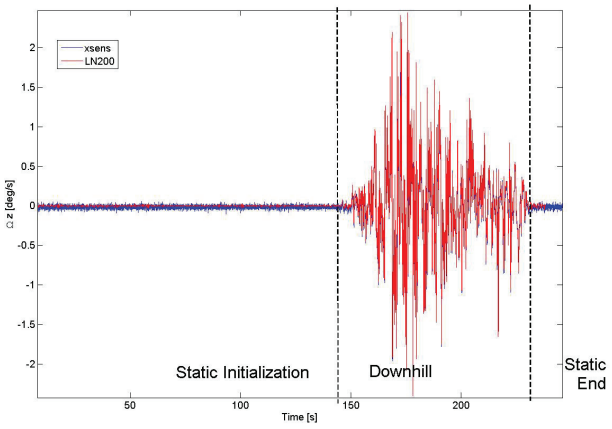

Fig. 6: Angular rotation rate around the z-axis.

Table 3 summarizes the result of a representative data set. It can be seen from the standard deviation that some biases estimated during the static initialization period are statistically irrelevant. On the other hand, the biases adjusted during the downhill are statistically meaningful and more precise. The scale factors for the accelerometers are statistically significant, whereas those for the gyroscopes proof to be insignificant. However, the correlation between the accelerometer biases and scale factors remains large (0.9 for the "horizontal" axis, 0.3 for the "vertical" axis).

Fig. 7 to Fig. 11 give examples of the estimated biases and scales factors for 3 MEMS sensors and 8 downhills. By comparing the time series of the biases estimated with and without scale factors during the dynamic portion of the downhill, it can be seen that the "bias-only" estimation provides similar values for all runs (Fig. 8 and

Fig. 10). The two methods do not provide statistically different results. On the other hand, if accelerometer biases and scale factors are adjusted, the results vary considerably between the tracks and seem to be correlated between the MEMS sensors (Fig. 7 and Fig. 9). It appears that the mean values of the biases and scale factors vary considerably between runs. This emphasizes the difficulty to separate them and thus to determine "constant" calibration parameters for accelerometers with statistical significance. Thus, the results of the accelerometer scale factors have to be analyzed with caution. However, the gyroscope biases seem to converge to more constant values with the two estimation methods, mainly because biases and scale factors decorrelate to a greater extent (Fig. 11 and Table 3).

Static Initialization	fx [m/s^2]	fy [m/s^2]	fz [m/s^2]	wx [deg/s]	wy [deg/s]	wz [deg/s]
Bias	0.008	0.171	0.020	-0.11	0.51	1.38
Std.	0.022	0.024	0.027	0.12	0.14	0.16

Downhill	fx [m/s^2]	fy [m/s^2]	fz [m/s^2]	wx [deg/s]	wy [deg/s]	wz [deg/s]
Bias	-0.049	0.039	-0.145	-0.21	0.38	1.39
Std. bias	0.003	0.003	0.009	0.01	0.01	0.01
Scale factor [-]	0.0046	-0.0533	-0.0223	-0.0051	-0.0118	0.0004
Std. scale factor [-]	0.0006	0.0009	0.0011	0.0212	0.0357	0.0250
Correlation [-]	0.93	0.32	0.98	0.31	0.43	0.14

Table 3: Estimated biases and scale factors during the static initialization and during the downhill of track #1 and MEMS sensor #1

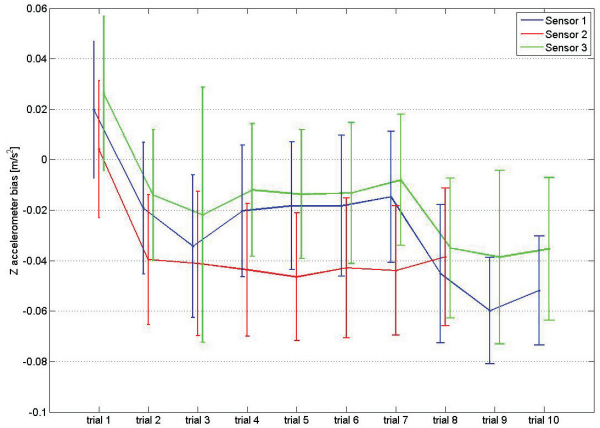

Fig. 7: Biases and standard deviations (1σ) adjusted during the static initialization of downhills #1 to #8 for the z-axis of 3 accelerometers

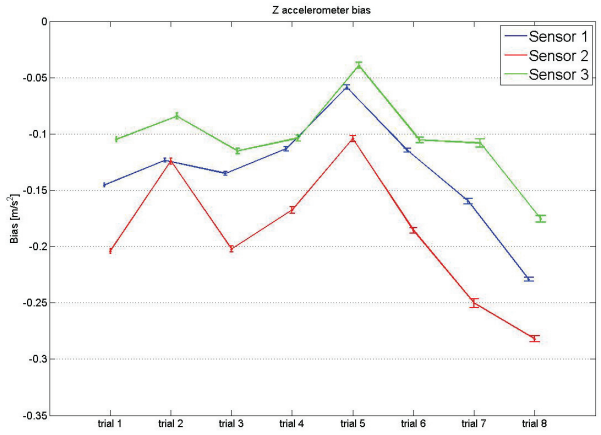

Fig. 8: Biases and standard deviations (1σ) adjusted during the downhills #1 to #8 for the z-axis of 3 accelerometers

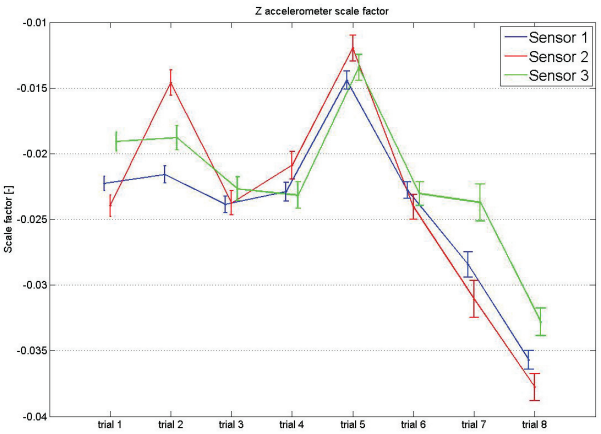

Fig. 9: Scale factors and standard deviations (1σ) adjusted during the downhills #1 to #8 for the z-axis of 3 accelerometers

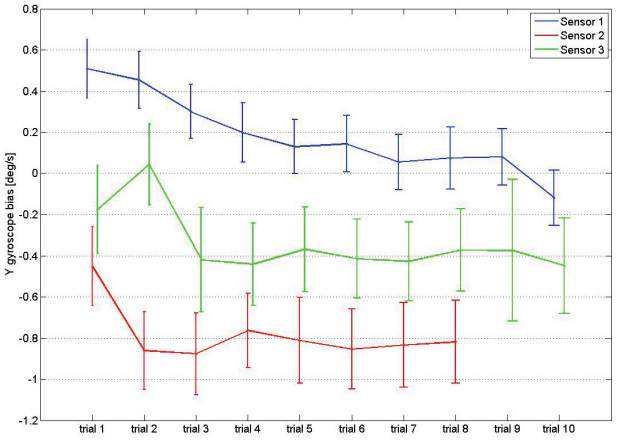

Fig. 10: Biases and standard deviations (1σ) adjusted during the static initialization of downhills #1 to #8 for the y-axis of 3 gyroscopes

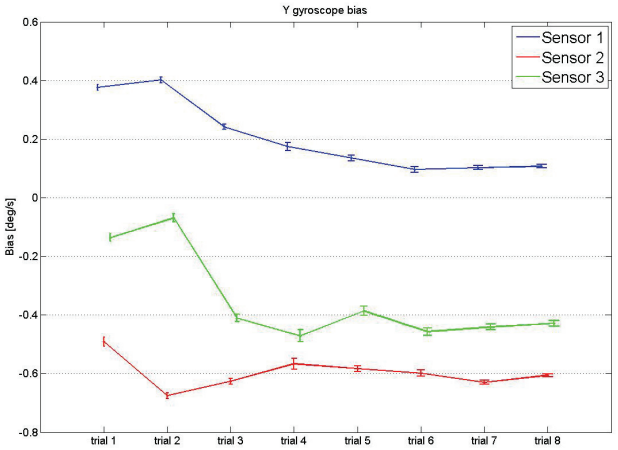

Fig. 11: Biases and standard deviations (1σ) adjusted during the downhills #1 to #8 for the y-axis of 3 gyroscopes

The biases deduced from the raw static signals are compared to those estimated by the EKF in Fig. 12 and Fig. 13. This comparison shows that the obtained differences are statistically insignificant.

We also studied the performance of the estimated biases and accelerometer scale factors fed back to the EKF. Either the biases estimated by the EKF or the calibrated biases from the raw data comparison were applied. The accelerometer scale factors were alternatively applied to the raw measurements. Table 4 illustrates the performance of the EKF for one representative downhill. By correcting the specific force measurements with the adjusted scale factors, the results are influenced negligibly. The differences turn up to be below centimeter-level and of a few hundredth of a degree for the orientation. When applying the calibrated biases instead of estimating them with the EKF, the results are worse. The differences are at the centimeter level and of the order of a few tenth of a degree.

The investigation has shown that the biases estimated by the EKF and those deduced from the comparison to the reference measurements were coherent. As shown in Table 4, applying the calibrated accelerometer scale factors does not improve the filter performance. This is most likely due to the large correlation with the estimated biases. Hence, extending the MEMS error model by constant scale factors does not lead to improved navigation performance of the integrated system.

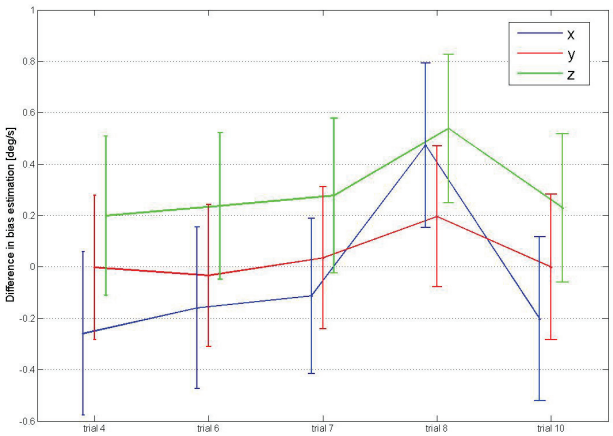

Fig. 12: Difference between the gyroscope biases estimated with the EKF and those deduced from the raw data comparison during the downhill (MEMS sensor #1). The error bar indicates the standard deviation of the difference (1σ).

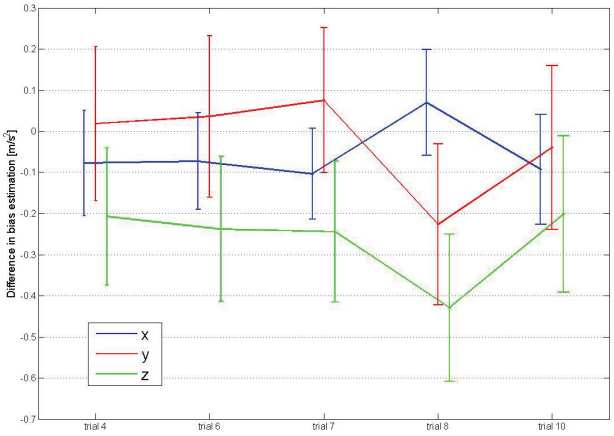

Fig. 13: Difference between the accelerometer biases estimated with the EKF and those deduced from the raw data comparison during the downhill (MEMS sensor #1). The error bar indicates the standard deviation of the difference (1σ).

Solution		1	2	3	4
Estimate bias with EKF		yes	yes	no	no
Apply calibrated biases		no	no	yes	yes
Apply calibrated accelerometer scale factors		no	yes	no	yes
RMS	N [m]	0.36	0.35	0.46	0.46
	E [m]	0.39	0.39	0.45	0.45
	h [m]	0.42	0.43	1.36	1.36
	rl [°]	0.87	0.95	2.67	2.68
	pt [°]	0.56	0.53	3.95	3.92
	hd [°]	0.70	0.91	1.11	1.10

Table 4: Accuracy of position and orientation as function of the applied biases and scale factors (downhill #10)

CONCLUSION AND PERSPECTIVES

The presented research aimed to investigate two alternative GPS/MEMS-IMU integration strategies and to evaluate the inertial error model of the L1 GPS/MEMS-IMU system for sports applications.

Various integration techniques were discussed. Extended (EKF) and unscented Kalman filters (UKF) haven been identified as the most appropriate methods for the sports application because of their rapid convergence, limited computational complexity and reasonable computational complexity. Unlike the EKF, the UKF does not require the linearization of the system model for state and covariance propagation. However, the experimental setup showed that the performance of both filter types was numerically equivalent. On the other hand, the UKF implementation tends to be computationally more expensive and numerically less stable than EKF. Nevertheless, UKF remains an efficient alternative for model evaluation and might proof interesting when non-linearities become more significant.

The inertial error model was evaluated through a comparison of the raw measurements between the tactical-grade reference IMU and the MEMS-IMU. It was shown that the specific force biases and scale-factors identified by this comparison during the dynamic portion of the downhill were strongly correlated. Furthermore, applying the estimated accelerometer scale factors to the raw MEMS measurement did not improve the performance of the EKF. The gyroscope scale factors could not be determined with statistical significance. Then, the application of the biases based on the raw signal comparison was compared to those estimated by the EKF. The difference of navigation performance was shown to be statistically insignificant for all the downhills which proves the adequacy of the adopted MEMS error model.

Future work will focus on the loosely coupled versus the closely coupled GPS/MEMS-IMU integration. The latter could bring benefits in this particular environment where satellite observations can be used even in the absence of GPS-position fix [21]. In addition, a setup of redundant MEMS-IMU will be investigated in order to reduce the noise in the navigation output parameters and detect IMU measurement errors [22].

ACKNOWLEDGMENTS

This research is financed by TracEdge, based at Chambéry, France.

REFERENCES

[1] A. Waegli and J. Skaloud, "Turning Point – Trajectory Analysis for Skiers," *InsideGNSS,* Spring 2007.

[2] J. How, N. Pohlman, and C.-W. Park, "GPS Estimation Algorithms for Precise Velocity, Slip and Race-track Position Measurements," in *SAE Motorsports Engineering Conference & Exhibition*, 2002.

[3] A. Waegli, "Assessment of GPS/MEMS-IMU Integration Performance in Ski Racing," in *ENC*, Geneva, Switzerland, 2007.

[4] M. Chansarkar, "Neural Networks in GPS Navigation," *GPS Solutions,* vol. 4, pp. 14-18, 2000.

[5] W. Abdel-Hamid, T. Abdelazim, N. El-Sheimy, and G. Lachapelle, "Improvement of MEMS-IMU/GPS performance using fuzzy modeling," *GPS Solutions,* vol. 10, 2006.

[6] A. Noureldin, A. El-Shafie, and M. R. Taha, "Optimizing neuro-fuzzy modules for data fusion of vehicular navigation systems using temporal cross-validation," *Engineering Applications of Artificial Intelligence,* vol. 20, pp. 49-61, 2007.

[7] Y. Yang and W. Gao, "An optimal adaptive Kalman filter," *Journal of Geodesy,* vol. 80, pp. 177-183, 2006.

[8] C. Hide, T. Moore, and M. Smith, "Adaptive Kalman Filtering for Low Cost INS/GPS," in *ION GPS*, Portland, OR, 2002.

[9] R. Van der Merwe, E. A. Wan, and S. I. Julier, "Sigma-Point Kalman Filter for Nonlinear Estimation and Sensor-Fusion - Applications to Integrated Navigation," in *AIAA Guidance, Navigation, and Control Conference and Exhibit*, 2004.

[10] E.-H. Shin, "Estimation Techniques for Low-Cost Inertial Navigation," in *Geomatic Engineering*. vol. PhD Calgary: University of Calgary, 2005.

[11] Y. Li, J. Wang, C. Rizos, P. Mumford, and W. Ding, "Low-cost tighly coupled GPS/INS integration based on a nonlinear Kalman filtering design," in *U.S. Institute of Navigation National Technical. Meeting*, Monterey, California, 2006, pp. 958-966.

[12] D. H. Titterton and J. L. Weston, *Strapdown inertial navigation technology*: Peter Peregrinus Ltd, 1997.

[13] A. Gelb, *Applied Optimal Estimation* vol. 14: MIT Press, 1994.

[14] D. Törnqvist, "Statistical Fault Detection with Applications to IMU Disturbances," in *Department of Electrical Engineering*: Linköping, Sweeden, 2006.

[15] R. Van der Merwe and E. A. Wan, "Efficient Derivative-Free Kalman Filters for Inline Learning," in *ESANN (European Symposium on Artificial Neural Networks) 2001*, Bruges, 2001.

[16] S. I. Julier and J. K. Uhlmann, "A General Method for Approximating Nonlinear Transformations of Probability Distributions," Department of Engineering Science, University of Oxford, Oxford 1996.

[17] R. Van der Merwe and E. A. Wan, "The Unscented Kalman Filter for Nonlinear Estimation," *IEEE,* 2000.

[18] V. Constantin, "Intégration GPS/MEMS-IMU basée sur un filtre de Kalman "sigma-point"," Lausanne: Ecole polytechnique fédérale de Lausanne, 2007.

[19] J. Nocedal and S. J. Wright, "Numerical optimization," New York: Springer Verlag, 1999.

[20] M. St-Pierre and D. Gingras, "Comparison between the unscented Kalman filter and the extended Kalman filter for the position estimation module of an integrated navigation information system," in *IEEE Intelligent Vehicles Symposium*, University of Parma, 2004.

[21] K. P. Schwarz, M. Wei, and M. Van Gelderen, "Aided Versus Embedded - A comparison of two approaches to GPS/INS integration."

[22] I. Colomina, M. Giménez, J. J. Rosales, M. Wis, A. Gómez, and P. Miguelsanz, "Redundant IMUs for Precise Trajectory Determination," in *XXth ISPRS Congress* Istanbul, 2004.